Geol. Mag. **150** (*4*), *2013, pp. 626–638.* © *Cambridge University Press 2013*
doi:10.1017/S0016756812000866

Polyphase transpressional development of a NNE-striking basement-cored anticline in the Xining Basin, northeastern Qinghai–Tibetan Plateau

J. ZHANG*† & D. CUNNINGHAM‡

*Institute of Geology, Chinese Academy of Geological Sciences, Beijing, China, 100037
‡Department of Environmental Earth Science, Eastern Connecticut State University, Willimantic, CT, USA

(*Received* 18 October 2011; *accepted* 17 September 2012; *first published online* 23 January 2013)

Abstract – The Xiaoxia anticline is a basement-cored fold in the northeastern Qinghai–Tibetan Plateau. It formed during the Middle–Late Cenozoic in a NNE-orientation oblique to prevailing WNW-striking thrusts in the surrounding region. The fold lies within the fault-bounded Xining Basin, which has behaved as a clockwise rotating and internally deforming block during the mid–late Tertiary. Proterozoic crystalline basement rocks and Jurassic–Cretaceous–Cenozoic terrestrial sediments exposed within the fold record three separate oblique-slip deformation events as determined by cross-cutting generations of faults and folds. The modern Xiaoxia anticline developed by: (1) outward-directed thrusting on the two fold limbs and, (2) oblique-slip thrusting on closely spaced minor NNE-striking faults that caused distributed uplift and passive shear folding of the sedimentary cover within the fold core. Tilted and thrusted river terraces on the flanks of the Xiaoxia anticline dated by optically stimulated luminescence and electron spin resonance indicate that folding has continued into the Late Quaternary (post-45.5 ± 5.5 ka) and therefore may still be active today. The development of the Xiaoxia anticline appears to be best explained in the context of the kinematic evolution of the Xining Basin's bounding strike-slip faults. Formation of the Xiaoxia anticline demonstrates that partitioned transpression in an evolving transpressional setting can invert intra-montane basins and produce basement-cored folds, thereby contributing to regional plateau uplift.

Keywords: basement-cored fold, Qinghai–Tibetan Plateau, oblique-slip thrust, transpression, Xining Basin.

1. Introduction

Basement-cored anticlines are prominent orogenic elements in many mountain ranges and understanding their development is important for studying the geometric and kinematic relationships between deep crustal displacements and contractional deformation of cover sediments (Stearns, 1978; Brown, 1988; Schmidt, Genovese & Chase, 1993; Stone, 1993; Miller & Mitra, 2011 and references therein). Most studies of basement-cored anticlines have focused on the Laramide foreland region of North America or the Sierras Pampeanas in Argentina (e.g. Jordan & Allmendinger, 1986; Schmidt, Genovese & Chase, 1993) and have generally used kinematic and mechanical models to explain the observed styles of deformation (Brown, 1988; Spang & Evans, 1988; Schmidt, Genovese & Chase, 1993; Narr & Suppe, 1994; Mitra & Mount, 1998; Tindall & Davis, 1999; Bump, 2003; Garcia & Davis, 2004). However, considerable debate surrounds the mechanisms of basement-cored fold growth and the range of tectonic settings in which such folds form (Brown, 1988; Paylor & Yin, 1993; English & Johnston, 2004; Garcia & Davis, 2004). Outstanding questions include: (1) whether contractional strain in the basement transfers to cover layers via a single fault zone (Mitra & Mount, 1998) or by closely spaced minor faults (Spang & Evans, 1988; Garcia & Davis, 2004; Otteman & Snoke, 2005); (2) what the role of structural reactivation is in the fold development (Huntoon, 1993; Marshak, Karlstrom & Timmons, 2000; Stone, 2002; Garcia & Davis, 2004); (3) whether the anticline formed in one stress field (Varga, 1993) or in several different stress fields involving separate deformational events (Wise & Obi, 1992), and, (4) in what tectonic settings do basement-cored folds form outside of 'thick-skinned' foreland regions.

In addition, the processes that have contributed to the development of the Qinghai–Tibetan Plateau are still poorly understood, especially in the northeastern corner of the plateau where structural trends are variable and where strike-slip faults, thrusts and folds have generated basinal compartments and thrusted ranges in a complex geomorphological arrangement that differs from the consistent NW-striking Qilian Shan fold-and-thrust belt to the NW (Fig. 1; England & Molnar, 1990; Tapponnier *et al.* 2001 and references therein; Yin *et al*. 2008). An important tectonic problem in the northeastern Tibetan Plateau region is how intermontane basins are structurally inverted within the context of overall plateau development (Tapponnier *et al*. 2001). In this study, we consider these issues through detailed examination of cross-cutting structures within a basement-cored anticline

† Author for correspondence: zhangjinem@sina.com

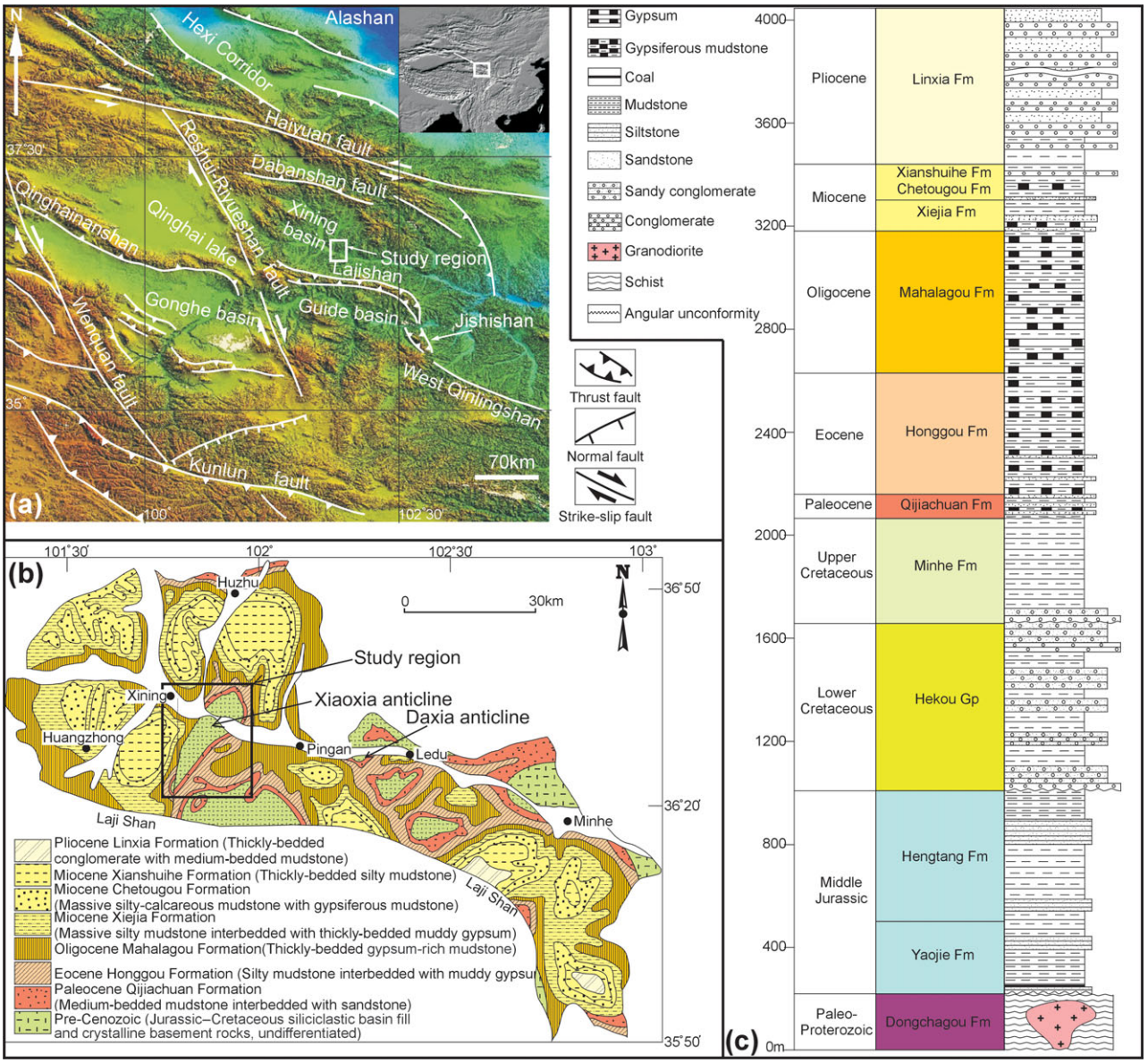

Figure 1. (a) Regional topography and major faults in the northeastern Qinghai–Tibetan Plateau. (b) Lithological map. (c) Stratigraphic column of Xining Basin, NE Tibet. Note location of NNE-striking Xiaoxia anticline.

that has evolved within an intraplate transpressional setting in the northeastern Qinghai–Tibetan Plateau.

2. Geological setting

The Xiaoxia anticline is located in the eastern Xining Basin located at the extreme northeastern corner of the Qinghai–Tibetan Plateau (Figs 1a, b, 2). The basin is a Mesozoic–Cenozoic clastic depocentre structurally bound by the Laji Shan Fault to the south, the Daban Shan Fault to the north and the Reshui–Riyue Shan Fault to the west (Fig. 1a). Proterozoic metamorphic rocks including grey staurolite-mica schist and garnet-biotite schist dated at 1250–1122 Ma (whole-rock Rb–Sr isochron age; BGMRQP, 1985, p. 17) and Early Palaeozoic fine- to medium-grained granodiorite dated at 434 ± 23 Ma (biotite K–Ar age) (BGMRQP, 1985, p. 153) directly underlie the basin. The granodiorite intrudes the schist, whereas grey-black lamprophyric dykes (0.1–2 m wide) locally intrude the granodiorite.

The Xining Basin fill includes Jurassic, Cretaceous and Cenozoic terrestrial sediments (Fig. 1b, c), which non-conformably overlie the basement rocks. Middle Jurassic sediments mainly occur on the northeastern limb of the Xiaoxia anticline, and Cretaceous sediments unconformably overlie the Jurassic section. The Cenozoic sediments conformably cover the Cretaceous rocks (Fig. 1b, c).

The Xiaoxia anticline is one of several basement-cored folds in the Xining Basin (Fig. 1b). The granodiorite and schist constitute the main rock types within the Xiaoxia anticline core, and are exposed over an area *c*. 9 km long and 0.2–2.3 km wide (Fig. 2). Structural relief between the anticlinal core and the basin floor to the west is about 4000–4500 m (Fig. 3).

https://doi.org/10.1017/S0016756812000866 Published online by Cambridge University Press

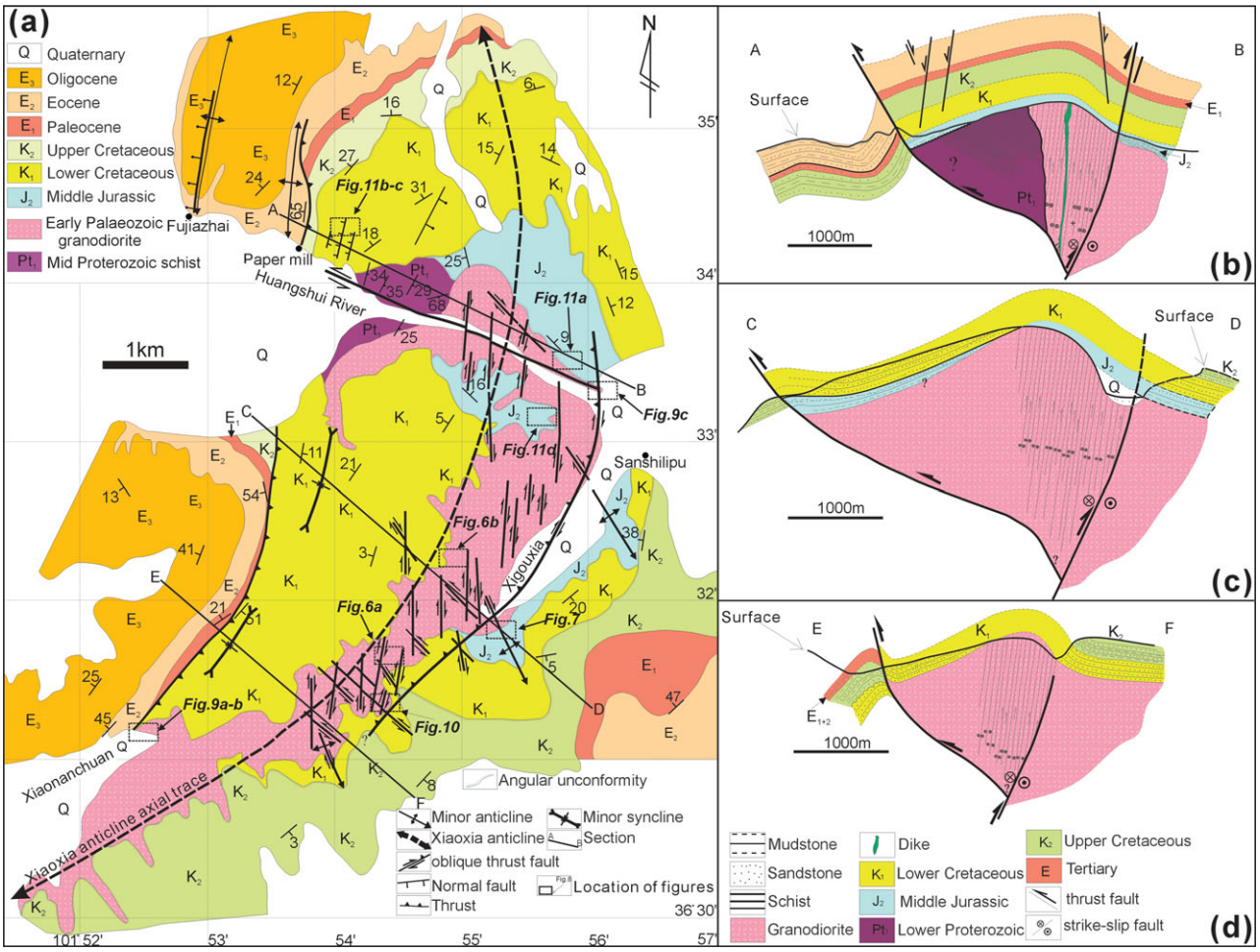

Figure 2. (a) Geological map of the Xiaoxia anticline within the Xining Basin. See Figure 1 for location. (b–d) NW–SE-striking sections across the Xiaoxia anticline.

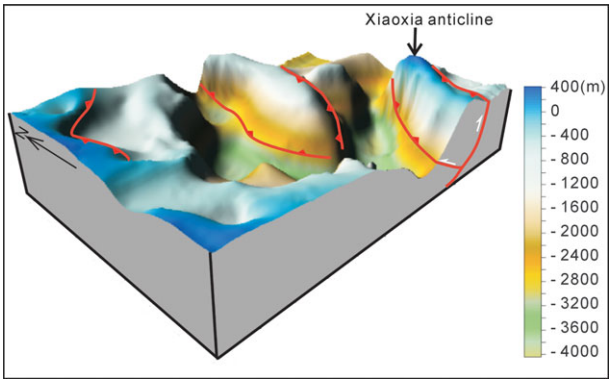

Figure 3. 3-D model of top-of-basement surface of the western Xining Basin. The red lines are interpreted to be NNE-striking faults bounding basement uplifts. The depth data are compiled from gravity modelling, drill holes and seismic reflection surveys in the Xining Basin (Wang *et al*. 2006). Depth scale indicates elevations above and below the modern land surface.

Owing to its recent development and good exposure, the Xiaoxia anticline provides an excellent opportunity to study the geometric and kinematic relationships between different generations of structures that formed in the basement and cover during fold development.

3. Structures in the basement

3.a. Structures in the basement schist

The schistose rocks of the Xiaoxia anticline experienced several deformation events. In addition to an early schistosity-forming event (1250–1122 Ma), the rocks contain minor folds and are cut by NNE-striking thrusts. The minor folds typically plunge southeast (163°/20°), oblique to the NNE strike of the main Xiaoxia anticline.

3.b. Structures in the granodiorite

The granodiorite within the fold core is intensely fractured and faulted. Several sets of faults were distinguished based on their attitudes and cross-cutting relationships (Figs 4, 5). From old to young, they consist of an early set of dextral oblique-slip thrusts (Set A), a cross-cutting set of sinistral oblique-slip thrusts (Set B) and late set of dextral oblique-slip thrusts (Set C) that cuts the other two fault sets. The most abundant faults are dextral oblique-slip thrusts (sets A and C; Figs 4a, 6a, c).

https://doi.org/10.1017/S0016756812000866 Published online by Cambridge University Press

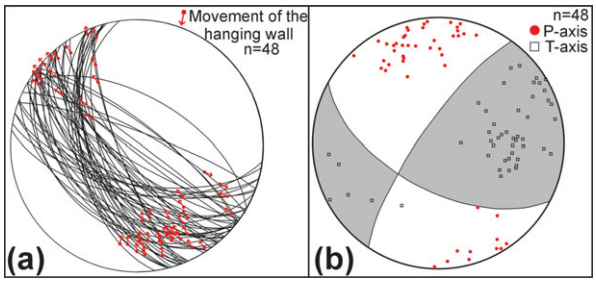

Figure 4. (Colour online) (a) Early dextral oblique-slip faults (Set A) and slickenlines in the basement. (b) Fault plane solution for Set A faults.

3.b.1. Early dextral oblique-slip thrusts (Set A)

Early dextral oblique-slip thrusts of Set A typically strike NW and dip SW with slickenline rakes ranging from 3° to 42° (Fig. 4a). These faults are common in the granodiorite on the SE limb of the Xiaoxia anticline (Fig. 2a). To the west of the Xigouxia Valley (Fig. 2a), faults of Set A cut both the granodiorite and the overlying NE-dipping Cretaceous sandstone and conglomerate. A fault plane solution indicates that the principal compression direction leading to the development of the faults of Set A was N–S striking (Fig. 4b).

On the SE limb of the Xiaoxia anticline, there are several kilometre-scale folds of Jurassic and Cretaceous strata plunging to the southeast (Fig. 2a). Faults of Set A in the granodiorite occur in the same location as these SE-plunging folds. To the west of Xigouxia Valley (Fig. 2a), the relationship between the faults of Set A and overlying sedimentary layers can be observed in a small quarry. At this location (36° 31′ 45″ N, 101° 55′ 15″ E), the faults cut both the granodiorite and the overlying NE-dipping Cretaceous sandstone and conglomerate indicating that the faulting postdates the Cretaceous rocks (Fig. 7a); some small NE-dipping normal faults are also present.

3.b.2. Sinistral oblique-slip thrusts (Set B)

In the granodiorite and schist in the fold core, NW-striking sinistral oblique-slip thrusts (Set B) are also present, but are less abundant than those of sets A and C (Fig. 8). An important example of this fault generation crops out along the Huangshui River where it cuts through the core of the Xiaoxia anticline. This fault zone contains abundant slip surfaces with slickenlines and kinematic indicators suggesting sinistral shearing (Fig. 2a), and slickenline rakes range from 11° to 35° (Fig. 8b). A fault plane solution for faults of Set

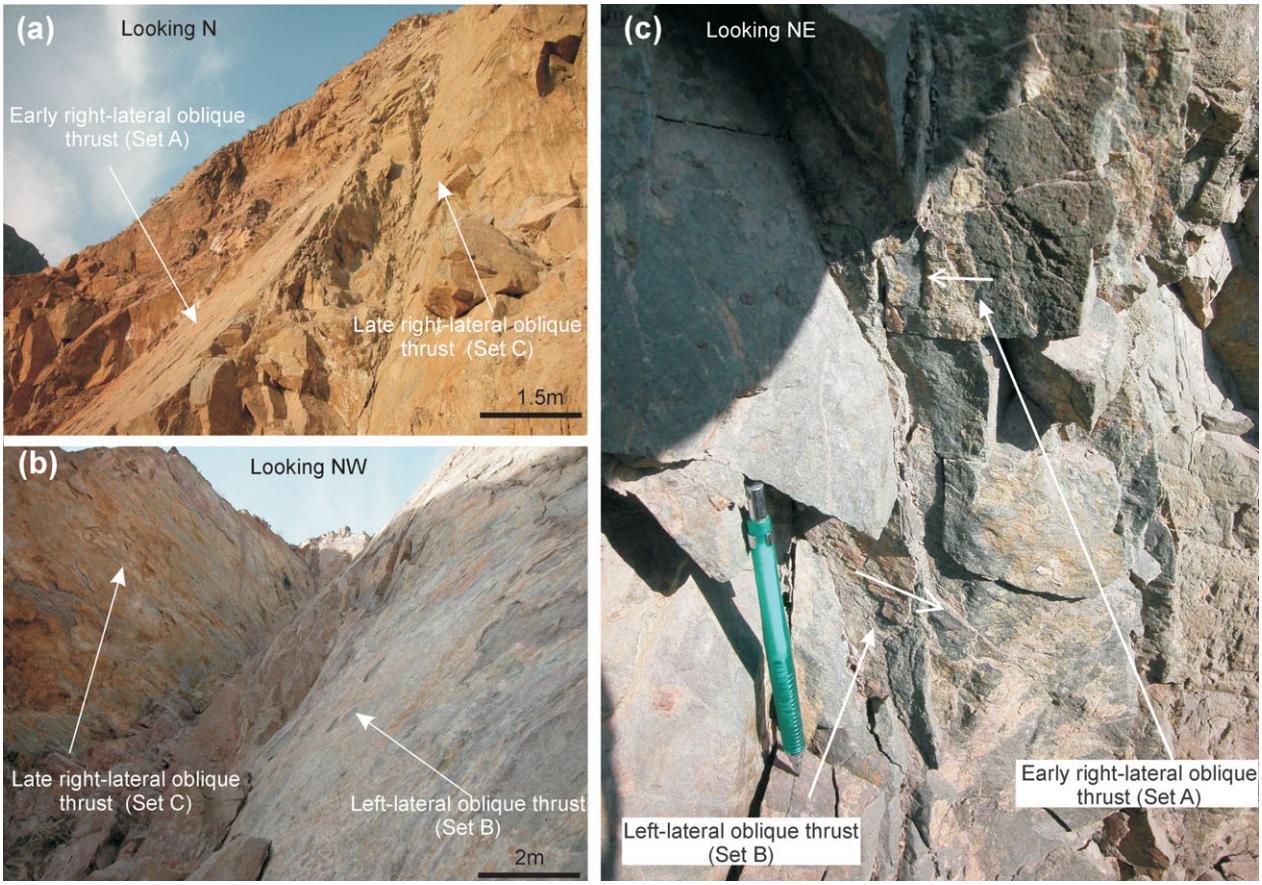

Figure 5. (Colour online) Photos showing cross-cutting relationships between different generations of brittle oblique-slip thrusts in the Xiaoxia basement. (a) Early dextral oblique-slip fault (Set A) cut by later dextral oblique-slip fault (Set C). (b) Sinistral oblique-slip fault (Set B) cut by late dextral oblique-slip fault (Set C). (c) Early dextral oblique-slip fault (Set A) cut by sinistral oblique-slip fault (Set B); the pen is 15 cm long. Small white arrows are parallel to fault plane slickenlines.

https://doi.org/10.1017/S0016756812000866 Published online by Cambridge University Press

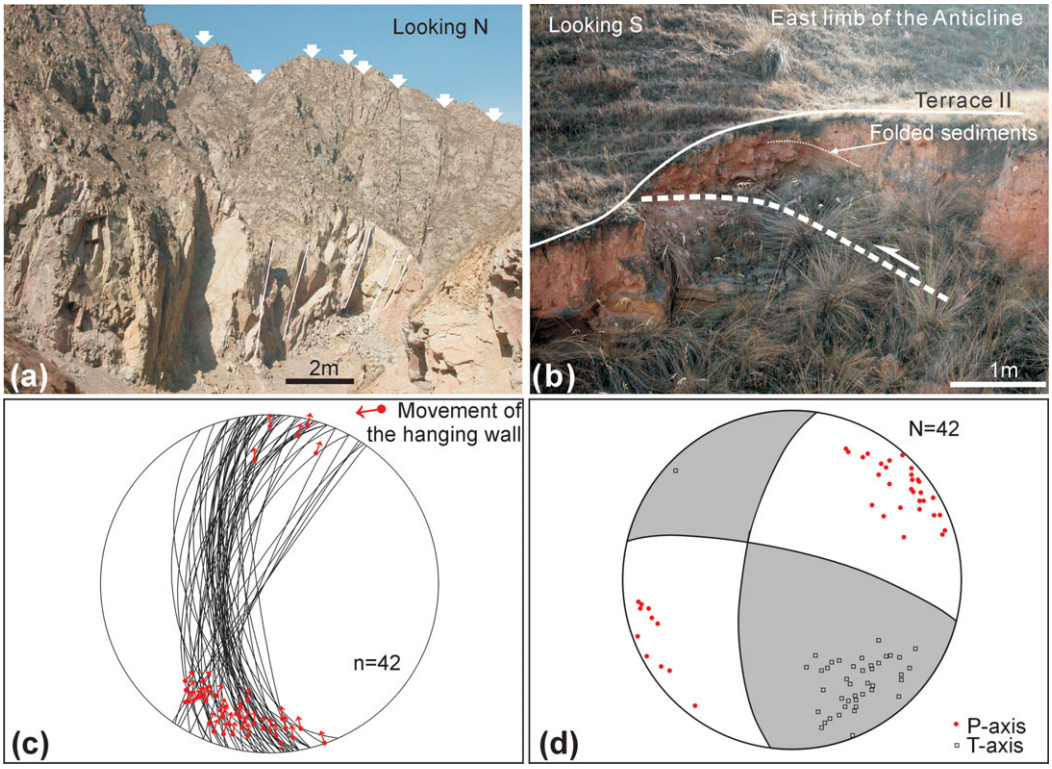

Figure 6. (Colour online) (a) Field views looking towards the N of closely spaced dextral oblique-slip faults in the granodiorite (arrows point to fault planes). (b) View S of a fold in Terrace II of the Huangshui River in the core of the Xiaoxia anticline (Fig. 2a) suggesting recent and possibly ongoing fault activity (Set C). (c) Late dextral oblique-slip faults (Set C) and slickenlines in the granodiorite. (d) Fault plane solution for Set C faults.

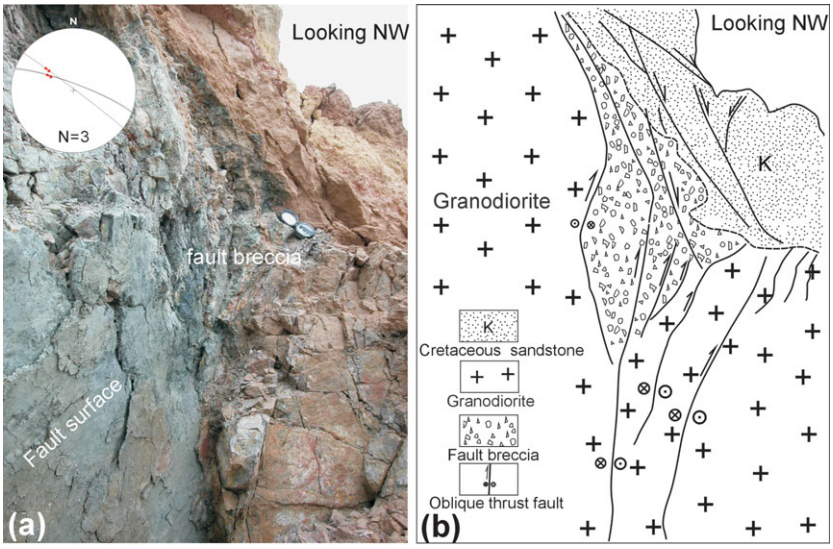

Figure 7. (Colour online) Photograph (a) and sketch (b) of early dextral oblique-slip fault (Set A) cutting the granodiorite and overlying Cretaceous sandstone in the east limb of the Xiaoxia anticline. The Brunton compass for scale in (a) is 16 cm long. Equal area stereographic projection (lower hemisphere) plot of faults shown in (a).

B shows that compression was NE–SW during their formation (Fig. 8c).

3.b.3. *Late dextral oblique-slip thrusts (Set C)*

Faults of Set C are closely spaced (*c*. 25–500 cm) in the granodiorite, separating many fault blocks (Fig. 6a). These faults are the most common brittle structures in the anticlinal core and provide good kinematic indicators. They mainly strike NNE and dip westerly at high angles (60–75°), and are sub-parallel to the regional fold hinge of the Xiaoxia anticline. Slickenline rakes range from 10° to 20° (Fig. 6c). Faults of Set C are most abundant in the fold core and east limb of the Xiaoxia anticline. However, fewer faults of this type are present in the west limb. Fault plane solutions indicate that NE–SW compression generated the dextral oblique-slip displacements (Fig. 6d).

https://doi.org/10.1017/S0016756812000866 Published online by Cambridge University Press

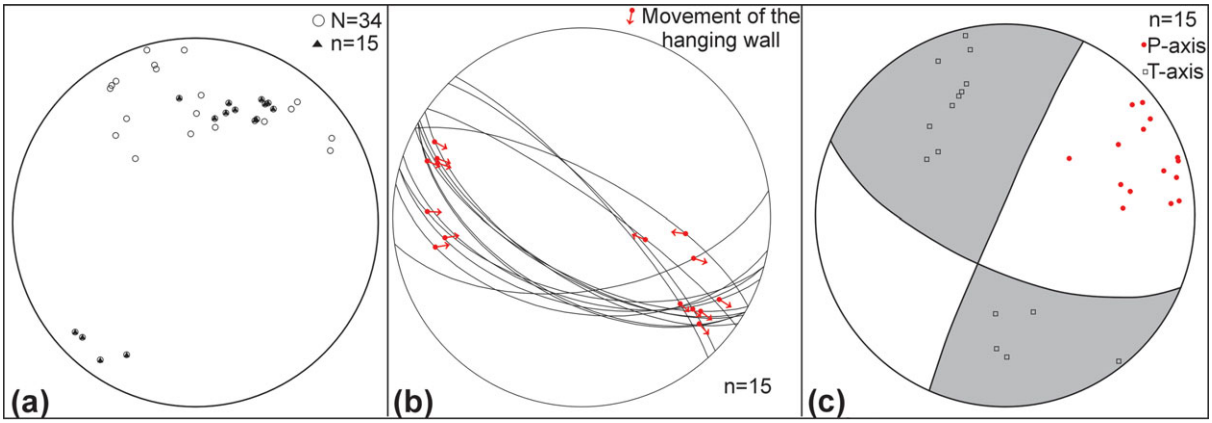

Figure 8. (Colour online) (a) Equal area lower hemisphere plot of sinistral faults (Set B) in the granodiorite (circles are all faults including faults without visible slickenlines; black triangles are faults of Set B that present visible slickenlines and clear kinematic indicators). (b) Sinistral oblique-slip faults (Set B) and slickenline orientations. (c) Fault plane solution for Set B faults.

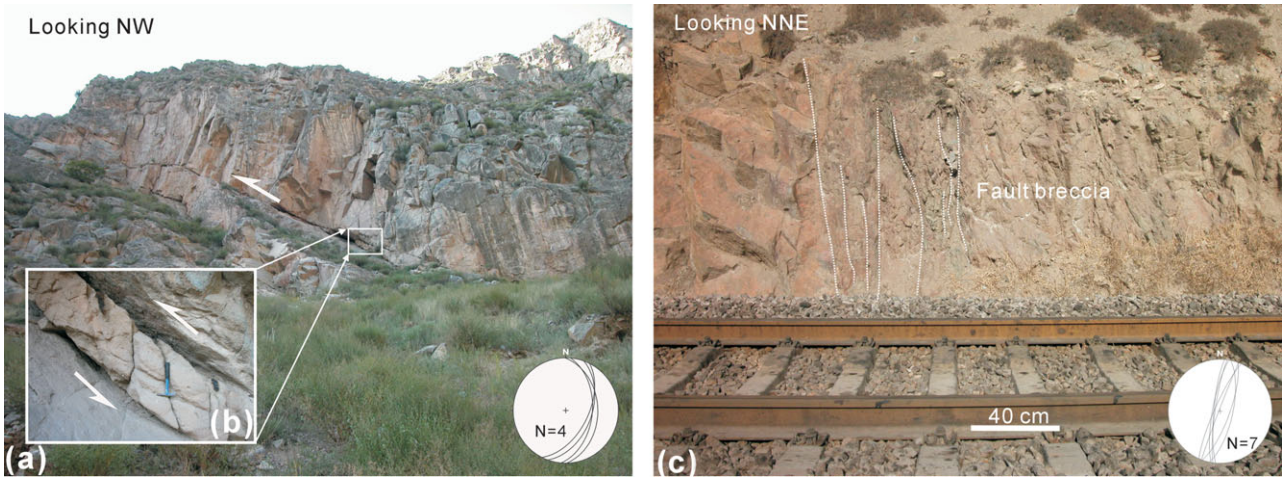

Figure 9. (Colour online) Major bounding faults of the Xiaoxia anticline. (a) Western bounding thrust zone showing its displacement sense; (b) equal area stereographic projection (lower hemisphere) plot of slip surfaces within fault zone; the hammer is 30 cm long. (c) Nearly vertical eastern bounding thrust with thick zone of fault brecciation, and equal area lower hemisphere stereoplot of slip surfaces within fault zone.

3.b.4. Bounding thrusts of the Xiaoxia anticline

Besides the abovementioned faults in the core of the Xiaoxia anticline, the western limb is cut by a major NNE-striking, E-dipping thrust which cuts the granodiorite (Figs 2, 9a, b) and Cretaceous–Cenozoic cover strata. Cretaceous strata are thrust over Eocene strata with at least 400 m of throw based on documented formational thicknesses and stratigraphic offset across the fault (Fig. 1c). East of Fujiazhai, this thrust crops out along a valley to the north of a paper mill (36° 34′ 30.7″ N, 101°53′ 47.3″ E; Fig. 2a, b). The hanging-wall is composed of thickly bedded Cretaceous sandstone and mudstone dipping to the west, and the footwall consists of thickly bedded mudstone, siltstone and gypsiferous sediments of the Eocene Honggou Formation. The footwall strata dip steeply to vertically near the fault, but away from the fault, the Honggou Formation strata are sub-horizontal. The Cenozoic strata in the hanging-wall are almost completely eroded off (Fig. 2a, b). The overall geometry suggests a fault-propagation anticline verging to the west (Fig. 2b–d). This major thrust cuts the whole NW limb of the Xiaoxia anticline and is therefore an important structure responsible for regional uplift (Fig. 2). The fault is also parallel to the metamorphic fabric in the nearest exposures of the schistose basement, raising the possibility that this major structure reactivates the schistosity at depth (Fig. 2a, b).

On the eastern limb, the eastern thrust is a near-vertical fault characterized by a 5 m thick fault breccia and gouge zone (Fig. 9c). To the south, this thrust is exposed in the Xigouxia Valley (Fig. 2a), where subsidiary splays of the main fault cut the overlying Cretaceous sandstone within a single 12 m long outcrop (Fig. 10a–c). The main thrust displaces the granodiorite over the Cretaceous sandstone. The amount of displacement is unquantified because of a lack of offset markers that can be correlated and because most of the fault zone is covered by Quaternary sediments.

https://doi.org/10.1017/S0016756812000866 Published online by Cambridge University Press

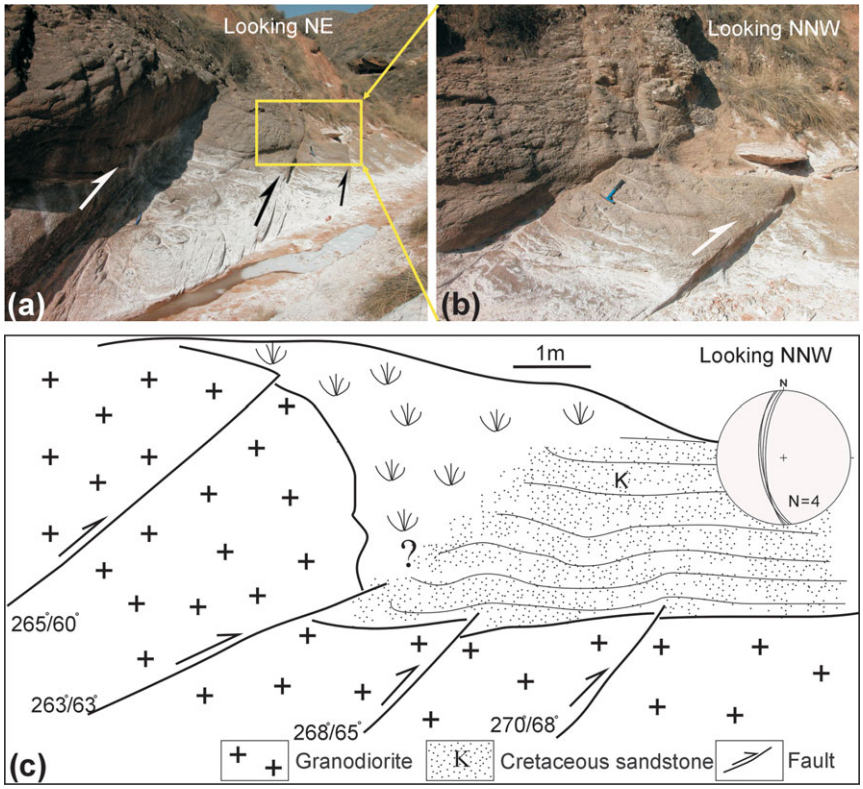

Figure 10. (Colour online) (a) Subsidiary splays of eastern bounding thrust that cuts basement and cover strata and contributes to uplift of the Xiaoxia fold core. Hammer for scale in (a) and (b) is 30 cm long. (b) Close-up view of yellow rectangular area shown in (a); (c) sketch looking NNW of the whole outcrop indicating dip amount and dip direction for four measured faults, and equal area stereographic projection (lower hemisphere) plot of faults. See Figure 2 for location.

4. Structures in the cover strata

4.a. Folds

Folds with two different trends and scales affect the cover strata. The larger-scale fold is simply the main NNE–SSW-trending Xiaoxia anticline. The regional geometry of Cenozoic strata across the fold is clearly anticlinal (Fig. 2a–d). On the eastern limb of the Xiaoxia anticline, Terrace III of the Huangshui River is tilted to the NNE (Fig. 11a). It occurs on the N-plunging part of the Xiaoxia anticline (Fig. 2a), which suggests that it is related to the development of the anticline.

Smaller-scale SE-plunging folds with *c*. 1.5 km wavelengths involving Jurassic and Cretaceous sediments occur on the eastern limb of the Xiaoxia anticline (Fig. 2a; see Section 3.b.1).

4.b. Normal faults in Cenozoic strata

In the Xiaoxia basement-cored anticline, there are also many mesoscale normal faults in Cenozoic strata, especially cutting the terraces of the Huangshui River (Fig. 11b–d). These normal faults mainly developed in the hanging walls of the two main bounding thrusts. On the western fold limb, Terraces IV–V of the Huangshui River are cut by almost vertical normal faults (Fig. 11b). Most of these normal faults dip to the west and are generally parallel to the strike of Set C thrusts and the overall anticline trend (Fig. 11b, c). The measured displacement on these faults ranges from 20 to 60 cm. On the eastern limb, normal faults also were observed, including non-degraded, 3 m high surface fault scarps (Fig. 11d), which may have formed during an earthquake in 1893 in the region (Tu *et al*. 1998).

5. Dating results

Because Quaternary river terraces on both limbs of the anticline are cut by major thrust faults or normal faults or are tilted by folding (Fig. 11a–d), samples were collected from Terraces II–V from both fold limbs to constrain the minimum age of anticline development. The dating was carried out at the State Key Laboratory of Earthquake Dynamics, Institute of Geology, China Earthquake Administration. For Terraces IV and V, samples were dated by electron spin resonance (ESR; Table 1), and for Terraces II and III, samples were dated by optically stimulated luminescence (OSL; Table 2). The samples used in the dating were all fine sands or silts collected above gravel beds from the different terraces (Tables 1, 2; Fig. 11a–d). The detailed sample preparation and OSL dating procedure including the different parameters used in the dating calculations are the same as those described by Wang, Lu & Li (2005). The ESR dating method is the same as that used by Yin *et al*. (2002).

Calculated ages for Terrace V ranges from 896 ± 89 ka BP to 1187 ± 118 ka BP, and for Terrace IV from

https://doi.org/10.1017/S0016756812000866 Published online by Cambridge University Press

Table 1. Terrace ages dated by ESR in the study region

No.	Sample name in the field	Sample name in the Lab	Latitude, Longitude	Terrace	Lithology	Method	Palaeodose (Gy)	Annual dose (Gy/ka)	Age (ka)
1	H4-IV-2	8412	36° 36.267′ N, 101° 59.364′ E	IV	Siltstone	ESR	1957 ± 195	3.35	584 ± 58
2	H1-IV-1	8416	36° 33.525′ N, 101° 58.229′ E	IV	Fine sands	ESR	2276 ± 227	3.61	630 ± 63
3	H2-IV-4	8417	36° 33.525′ N, 101° 58.229′ E	IV	Siltstone	ESR	2005 ± 200	3.42	586 ± 58
4	WXX-V-1	8407	36° 33.905′ N, 101° 54.494′ E	V	Siltstone	ESR	2748 ± 274	2.91	944 ± 94
5	EXX-V-1	8410	36° 34.281′ N, 101° 54.630′ E	V	Fine sands	ESR	4371 ± 737	3.68	1187 ± 118
6	EXX-V-2	8411	36° 34.281′ N, 101° 54.630′ E	V	Fine sands	ESR	2655 ± 265	2.96	896 ± 89

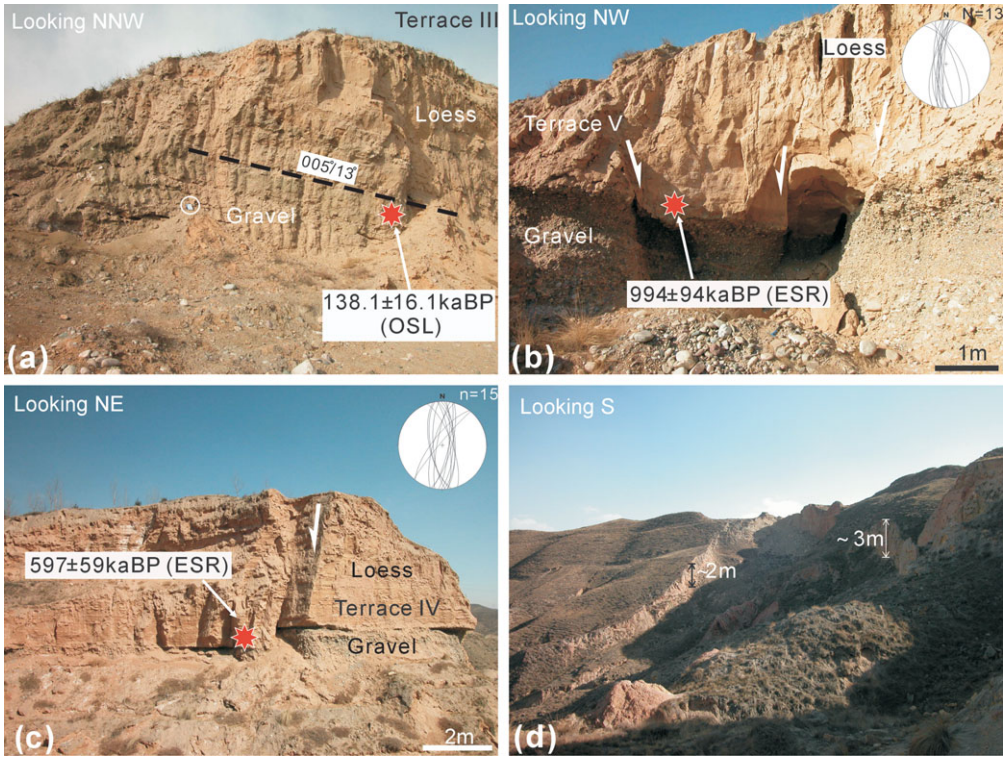

Figure 11. (Colour online) (a) View NNW of tilted Terrace III of the Huangshui River at the N-plunging end of the Xiaoxia anticline. Red star is the sample location for OSL dating and the field notebook shown for scale is 22 cm long. (b) View NW of normal faults cutting Terrace V of the Huangshui River on the western limb of the anticline. Equal area stereographic projection (lower hemisphere) of measured faults is also shown. Red star is the sample location for ESR dating. (c) View NE of normal faults cutting Terrace IV of the Huangshui River on the western limb of the anticline and equal area stereographic projection (lower hemisphere) of measured faults. Red star is the sample location for ESR dating. (d) View S of normal fault scarp on eastern limb of the Xiaoxia anticline possibly suggesting Holocene–Recent co-seismic surface faulting (see Figure 2 for locations).

584 ± 58 ka BP to 630 ± 63 ka BP. Terrace III was dated at 138.1 ± 16.1 ka BP and Terrace II was dated at 45.5 ± 5.5 ka BP to 64.2 ± 7.7 ka BP (Tables 1, 2). These age ranges for different terraces are similar to previously published ages for terraces of the Huangshui River west of this study region (Li *et al*. 1996; Lu *et al*. 2004).

6. Discussion and conclusions

6.a. Ages of different sets of faults, major thrusts and normal faults

Structures in the granodiorite and overlying sediments and their cross-cutting relationships reveal a sequence of deformation events that can account for the development of the basement-cored Xiaoxia anticline.

The older oblique-slip thrusts (Set A) are dominantly NW-striking (Fig. 4a). This fault array formed under N–S compression (Fig. 4b) and affects Jurassic and Lower Cretaceous cover sediments, but not Upper Cenozoic strata (Fig. 2a). The close spatial relationship between SE-plunging folds on the eastern limb of the Xiaoxia anticline and NW-striking early dextral oblique-slip thrusts (Set A), suggests that they may be kinematically related; the folds possibly formed as strike-slip related en échelon folds or as a passive response to oblique-slip thrusting at depth (Figs 2, 7).

Younger sinistral oblique-slip thrusts (Set B) which formed under NE–SW compression (Fig. 8c) cut the oblique-slip thrusts of Set A (Fig. 5c), but are in turn cross-cut by the oblique-slip thrusts of Set C (Fig. 5b), which cut not only all overlying Mesozoic–Cenozoic strata including at least Terrace II of the Huangshui

https://doi.org/10.1017/S0016756812000866 Published online by Cambridge University Press

Table 2. Terrace age dated by OSL in the study region

No.	Sample name in the field	Sample name in the Lab	Latitude, Longitude	Terrace	Lithology	Method	Depth (m)	Alpha count rates (Counts/ks)	K (%)	Measured water content (%)	Dose rate (Gy/ka)	Equivalent dose (Gy)	Age (ka)
1	WXX-I-1	LEDL09-16	36° 33.905′ N, 101° 54.494′ E	II	Fine sands	OSL (SMAR fine-grained quartz)*	3	9.23 ± 0.24	1.6	1	3.82 ± 0.38	174.0 ± 12.0	45.5 ± 5.5
2	WXX-I-2	LEDL09-17	36° 33.905′ N, 101° 54.494′ E	II	Fine sands	OSL (SMAR fine-grained quartz)*	3	8.02 ± 0.23	1.66	1	3.62 ± 0.36	232.9 ± 15.4	64.2 ± 7.7
3	EXX-II-1	LEDL09-18	36° 33.690′ N, 101° 55.406′ E	III	Fine sands	OSL (SMAR fine-grained quartz)*	3.5	7.08 ± 0.21	1.62	1	3.37 ± 0.34	465.6 ± 28.5	138.1 ± 16.1
4	WXX-II-2	LEDL09-19	36° 33.905′ N, 101° 54.494′ E	III	Fine sands	OSL (SMAR fine-grained quartz)*	3.5	8.88 ± 0.23	1.68	5	3.82 ± 0.38	> 450	> 120

*SMAR (Simplified Multiple Aliquot Regenerative), the detailed meaning and method of SMAR can be found in Wang *et al.* (2005).

River in the core (Fig. 6b), but also faults of Set A in the basement (Fig. 5a). Therefore, this youngest array of NNE-striking dextral oblique-slip thrusts (Set C) represents the most recent deformation event in the anticline, and may be still active.

The two major thrusts that cut the limbs of the Xiaoxia anticline were observed to cut Cenozoic sediments (Fig. 2) and faults of sets A and B, but not Set C faults. Thus they are interpreted to have formed during or before the formation of the Set C faults.

The normal faults that cut the Quaternary terraces on the two limbs of the Xiaoxia anticline appear to be the youngest fault generation because they are only observed cutting the youngest Quaternary cover strata such as the mid–late Quaternary Huangshui terraces. For this reason, we interpret these normal faults to have been caused by outer-arc stretching during continued uplift and fold growth of the Xiaoxia anticline.

These documented cross-cutting field relationships indicate that faults of Set C, the two major thrust faults and young normal faults were mainly developed in the Late Cenozoic period. However, faults of sets A and B are older and therefore may have been active earlier in the Tertiary. Their depth of formation is unconstrained, but they are likely to be shallow upper crustal faults (active at < 4 km depth) because they cut un-metamorphosed Cretaceous sediments which are overlain by a maximum of 2–4 km of post-Cretaceous Tertiary infill deposited during slow protracted periods of basin subsidence (Fig. 1; Horton *et al*. 2004).

6.b. Mechanism of folding within the Xiaoxia anticline

The field observations indicate that at first-order, the Xiaoxia anticline is bound by two major NNE-striking thrusts, which have played a major role in elevating the fold's basement core (Fig. 2b–d).

In addition, in the fold core, thrust components of displacement on the abundant and widely distributed Set C dextral oblique-slip thrusts are likely to have also contributed to overall fold growth. The cumulative displacements on these minor faults are unknown, but because they occur within the fold core and strike parallel to the hinge, they also generated some uplift and anticlinal arching of the NNE-striking Xiaoxia anticline. Regionally, the top of the basement outcrops is a convex-up curved surface (Fig. 2); the nonconformity is cut by a large number of minor faults with components of dip-slip displacement. Thus the behaviour of the basement and cover strata is like that of a passive shear fold. The basement has deformed as a fold at a large scale because of cumulative minor displacements on abundant mesoscale faults. Cover sediments responded to inhomogeneous shear from below by bending and local faulting.

6.c. Evolutionary model linking faults in the Xiaoxia anticline with basin-bounding faults

Although the Xiaoxia anticline formed within the Xining Basin centre and cannot be linked at the

https://doi.org/10.1017/S0016756812000866 Published online by Cambridge University Press

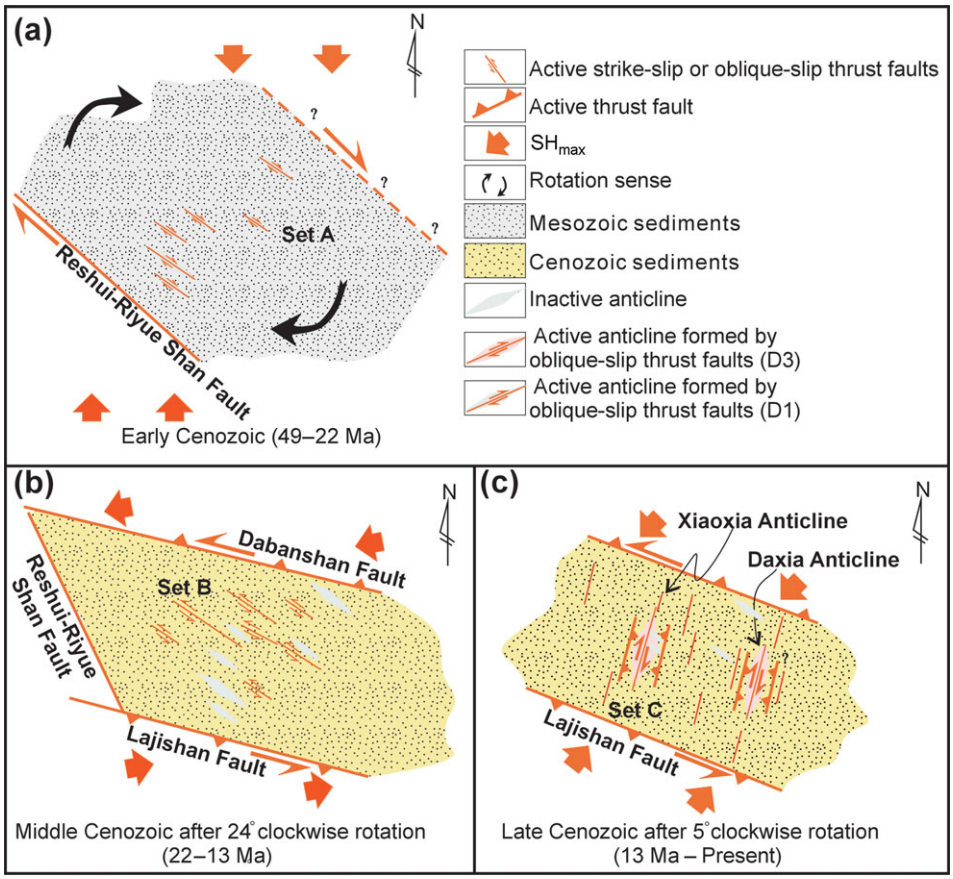

Figure 12. Three-stage evolutionary model for development of the Xiaoxia anticline. (a) Early–Middle Cenozoic period (49–22 Ma). (b) Middle–Late Cenozoic period (22–13 Ma). (c) Late Cenozoic period (13 Ma – Present).

surface with deforming belts that bound the basin such as the Dabanshan and Lajishan to the north and south, respectively, palaeomagnetic data from Dupont-Nivet *et al*. (2004) indicate that the basin interior has rotated in a clockwise sense since the mid-Tertiary, and therefore the evolution of the basin interior is likely to be related to the bounding structures that accommodated the block rotation. Thus, we prefer an evolutionary model for the Xiaoxia anticline that connects with the wider tectonic development of the Xining Basin block.

Generally, the deformed Upper Cenozoic strata in the anticlinal ridge indicate that the Xiaoxia anticline mainly developed during the Late Cenozoic period (Fig. 2). Based on the above interpretations, and combined with the palaeomagnetic study of the Xining Basin by Dupont-Nivet *et al*. (2004) and the uplift ages of basin-bounding mountain ranges in the study region (Lease *et al*. 2007, 2011; Hough *et al*. 2011), a three-stage evolutionary model for the development of the Xiaoxia anticline is presented that accounts for the different generations of structures documented in the basement and cover and which takes into consideration the regional tectonic context (Fig. 12).

During stage 1 (49–22 Ma; Fig. 12a), dextral displacements along NW-striking regional dextral fault systems such as the Reshui–Riyue Shan Fault and Wenquan Fault to the west of the Xiaoxia anticline (Fig. 1a) drove clockwise block rotation and caused initiation (and/or reactivation) of NW-striking basement structures in dextral oblique-slip mode (Set A). Dextral displacements along NW-striking faults may have been related to approximately N–S SH_{max} (maximum horizontal compressive stress) acting on NW-striking basement block boundaries around the NE Tibetan Plateau margin and diffuse dextral shear along the eastern margin of the Tibetan Plateau (England & Molnar, 1990).

During stage 2 (22–13 Ma; Fig. 12b), following 24° of clockwise rotation of the Xining Basin (Dupont-Nivet *et al*. 2004), NE-directed SH_{max} drove sinistral displacements along the northern and southern basin-bounding faults (Dabanshan and Lajishan faults, respectively; Fig. 8c; cf. Lease *et al*. 2011). During this stage, the Xining Basin compartment developed sinistral displacements on NW-striking faults (Set B) that were possibly synthetic faults (P shear faults) related to the bounding sinistral Dabanshan and Lajishan faults.

During stage 3 (13 Ma – Present; Fig. 12c), SH_{max} changed from the previous NNE direction to NE (Fig. 6d), which is also similar to the direction of SH_{max} suggested by Lease *et al*. (2011) for this period. Outward-directed thrusting on the limbs of the evolving Xiaoxia anticline developed in addition to distributed displacements on NNE-striking dextral oblique-slip

https://doi.org/10.1017/S0016756812000866 Published online by Cambridge University Press

thrusts (Set C). These densely developed NNE-striking basement structures were favourably oriented for continued dextral oblique-slip thrust displacements in response to continued sinistral strike-slip displacements along the basin-bounding Dabanshan and Lajishan faults and continued NE-directed regional SH_{max} driven by India's continued NE indentation further south (Fang *et al*. 2005; Lease *et al*. 2011). Therefore, during the Late Cenozoic, the Xining Basin crust in the Xiaoxia region was dominated by antithetic bookshelf-style strike-slip faulting with thrusting components similar to what has been reported for other internally deforming strike-slip bounded compartments (e.g. Newberry *et al*. 1995; Leonard, Mazzotti & Hyndman, 2008). It is worth noting that NNE-trending faults have also been documented by seismic reflection surveys elsewhere in the Xining Basin basement (Fig. 3). The initial Late Jurassic – Cretaceous stage of Xining Basin sedimentary accumulation is interpreted to be extensional fault-controlled (Horton *et al*. 2004), thus raising the possibility that some Set C faults originated as older normal faults that were later reactivated in dextral oblique-slip mode.

6.d. Transpressional deformation and NE Tibetan plateau growth

Geological observations and structural data from the Xiaoxia anticline indicate that the fold has some geometrical characteristics reminiscent of flower structures, including outward-directed thrusts cutting the fold limbs and an inner zone dominated by steep faults with strike-slip and oblique-slip components (Harding, 1985; Schreurs & Colletta, 1998). Activation of many small faults in the Xiaoxia fold core may be due to partitioning of the regional transpressional strain between the two major outward-directed bounding thrusts and smaller oblique-slip and strike-slip faults.

The Xiaoxia anticline differs from other basement-cored folds such as the Rawlins uplift in the Laramide foreland region (Otteman & Snoke, 2005) and the Sierra de Hualfin uplift in NW Argentina (Garcia & Davis, 2004), which are more dominated by contractional dip-slip displacements in an orogenic foreland. However, the Xiaoxia basement-cored fold and the classic Laramide thick-skinned uplifts both developed in an intracontinental setting as a crustal response to compressional stresses derived from a distant convergent plate margin. In both settings, topographic inversion of basin sediments occurred as the orogen grew outward and the crust thickened. In the case of the Laramide uplifts, flat-slab subduction and a thin sedimentary veneer in a distant foreland setting promoted crustal shortening that involved deep-seated thrusts (Dickinson & Snyder, 1978; Allmendinger *et al*. 1987). However, the Xiaoxia anticline is different in that it is forming within a region that is developing into a major plateau and therefore it is possible that deeper crustal displacements and lower crustal thickening in the plateau are also coupled with the upper crustal transpressional deformation within the Xining Basin (Royden *et al*. 1997). In addition, the structural relationships exposed in the Xiaoxia anticline indicate that basin inversion and 4–5 km of rock uplift were caused by oblique-slip deformation within a basin that occurs within a larger region characterized by thrusting of basement blocks, sedimentary infill of large intra-montane basins and lateral displacements along regional strike-slip fault systems (Meyer *et al*. 1998).

In the Xining Basin, there are other basement uplifts in addition to the Xiaoxia anticline that act to structurally compartmentalize the crust. These uplifts include the Daxia anticline and other un-named NNE-striking uplifts that are revealed by the geological and top-to-basement map (Figs 1b, 3). Also, in the wider Xining Basin region (including the Minhe sub-basin and Ledu sub-basin, Fig. 1b), there are other NNE–SSW-striking active oblique-slip thrusts that bound basement uplifts (Tu *et al*. 1998). Thus, the complex internal structure of the Xining Basin indicates that the uplift of the northeastern Qinghai–Tibetan Plateau is not simply due to NE-directed thrusting associated with the Qilian Shan, but also involves a more complex history of polyphase transpressional faulting, basin inversion and basement-cored fold development.

Acknowledgements. The authors are grateful to Dr Chen Hongyi and Prof. Li Jingyi and anonymous reviewers who provided many constructive suggestions. We also thank Dr Liu Jinfeng of State Key Laboratory of Earthquake Dynamics, Institute of Geology, China Earthquake Administration for dating the samples used in this study. This research was funded by Scientific Special Projects of the Institute of Geology, Chinese Academy of Geological Sciences (No. J1121).

References

ALLMENDINGER, R. W., NELSON, K. D., POTTER, C. J., BARAZANGI, M., BROWN, L. D. & OLIVER, J. E. 1987. Deep seismic reflection characteristics of the continental crust. *Geology* **15**, 304–10.

BROWN, W. G. 1988. Deformational style of Laramide uplifts in the Wyoming foreland. In *Interaction of the Rocky Mountain Foreland and the Cordilleran Thrust Belt* (eds C. J. Schmidt & W. J. Perry), pp.1–25. Geological Society of America Memoir no. 171.

BUMP, A. P. 2003. Reactivation, trishear modeling, and folded basement in Laramide uplifts: implications for the origins of intra-continental faults. *Geological Society of America Today* **13**, 4–10.

BUREAU OF GEOLOGICAL AND MINERAL RESOURCES OF QINGHAI PROVINCE (BGMRQP). 1985. *Regional Geological Survey Reports of Duoba, Xining, Tianjiazhai and Gaodian, Qinghai Province, P.R. China*. Geological Publishing House, 199 pp.

DICKINSON, W. R. & SNYDER, W. S. 1978. Plate tectonics of the Laramide orogeny. In *Laramide Folding Associated with Block Faulting in the Western United States* (ed. V. Matthews), pp. 355–66. Geological Society of America Memoir no. 151.

DUPONT-NIVET, G., HORTON, B. K., BUTLER, R. F., WANG, J., ZHOU, J. & WAANDERS, G. L. 2004. Paleogene clockwise tectonic rotation of the Xining-Lanzhou region,

https://doi.org/10.1017/S0016756812000866 Published online by Cambridge University Press

northeastern Tibetan Plateau. *Journal of Geophysical Research* **109**, B04401, doi:10.1029/2003JB002620, 13 pp.

ENGLAND, P. C. & MOLNAR, P. 1990. Right-lateral shear and rotation as the explanation for strike-slip faulting in eastern Tibet. *Nature* **344**, 140–2.

ENGLISH, J. M. & JOHNSTON, S. T. 2004. The Laramide Orogeny: what were the driving forces? *International Geology Review* **46**, 833–8.

FANG, X., YAN, M., ROB, V., DAVID, K. R., SONG, C. H., JOSEP, M. P., GAO, J. P., NIE, J. S. & DAI, S. 2005. Late Cenozoic deformation and uplift of the NE Tibetan Plateau: evidence from high-resolution magnetostratigraphy of the Guide Basin, Qinghai Province, China. *Geological Society of America Bulletin* **117**, 1208–25.

GARCIA, P. E. & DAVIS, G. H. 2004. Evidence and mechanisms for folding of granite, Sierra de Hualfin basement-cored uplift, northwest Argentina. *American Association of Petroleum Geologists Bulletin* **88**, 1255–76.

HARDING, T. P. 1985. Seismic characteristics and identification of negative flower structures, positive flower structures and positive structural inversion. *Association of Petroleum Geologists Bulletin* **69**, 582–600.

HORTON, B. K., DUPONT-NIVET, G., ZHOU, J., WAANDERS, G. L., BUTLER, R. F. & WANG, J. 2004. Mesozoic–Cenozoic evolution of the Xining-Minhe and Dangchang basins, northeastern Tibetan Plateau: magnetostratigraphic and biostratigraphic results. *Journal of Geophysical Research* **109**, B04402, doi: 10.1029/2003JB002913, 15 pp.

HOUGH, B. G., GARZIONE, C. N., WANG, Z. C., LEASE, R. O., BURBANK, D. W. & YUAN, D. Y. 2011. Stable isotope evidence for topographic growth and basin segmentation: implications for the evolution of the NE Tibetan plateau. *Geological Society of America Bulletin* **123**, 168–85.

HUNTOON, P. W. 1993. Influence of inherited Precambrian basement structure on the localization and form of Laramide monoclines, Grand Canyon, Arizona. In *Laramide Basement Deformation in the Rocky Mountain Foreland of the Western United States* (eds C. J. Schmidt, R. B. Chase & E. A. Erslev), pp. 243–56. Geological Society of America Special Paper no. 280.

JORDAN, T. E. & ALLMENDINGER, R. W. 1986, The Sierras Pampeanas of Argentina; a modern analogue of Rocky Mountain foreland deformation, *American Journal of Science* **286**, 737–64.

LEASE, R. O., BURBANK, D. W., GEHRELS, G. E., WANG, Z. C. & YUAN, D. Y. 2007. Signatures of mountain building: detrital zircon U/Pb ages from northeastern Tibet. *Geology* **35**, 239–42.

LEASE, R. O., BURBANK, D. W., CLARK, M. K., FARLEY, K. A., ZHENG, D. & ZHANG, H. 2011. Middle Miocene reorganization of deformation along the northeastern Tibetan Plateau. *Geology* **39**, 359–62.

LEONARD, L., MAZZOTTI, S. & HYNDMAN, R. 2008. Deformation rates estimated from earthquakes in the northern Cordillera of Canada and eastern Alaska. *Journal of Geophysical Research* **113**, B08406, doi: 10.1029/2007JB005456, 18 pp.

LI, J. J., FANG, X. M., MA, H. Z., ZHU, J. J., PAN, B. T. & CHEN, H. L. 1996. Geomorphological and environmental evolution in the upper reaches of the Yellow River during the late Cenozoic. *Science in China (Earth Science)* **39**, 380–90.

LU, H. Y., AN, Z. S., WANG, X. Y., TAN, H. B., ZHU, R. X., MA, H. Z., LI, Z., MIAO, X. D. & WANG, X. Y. 2004. Geomorphological evidences of staged uplift of northeastern Qinghai-Tibetan Plateau during latest 14Ma. *Science in China (Series D)* **34**, 855–64.

MARSHAK, S., KARLSTROM, K. & TIMMONS, J. M. 2000. Inversion of Proterozoic extensional faults: an explanation for the pattern of Laramide and Ancestral Rockies intracratonic deformation, United States? *Geology* **28**, 735–8.

MEYER, B., TAPPONNIER, P., BOURJOT, L., METIVIER, F., GAUDEMER, Y., PELTZER, G., GUO, S. & CHEN, Z. 1998. Crustal thickening in Gansu-Qinghai, lithospheric mantle subduction, and oblique, strike-slip controlled growth of the Tibet Plateau. *Geophysical Journal International* **135**, 1–47.

MILLER, J. F. & MITRA, S. 2011. Deformation and secondary faulting associated with basement-involved compressional and extensional structures. *American Association of Petroleum Geologists Bulletin* **95**, 675–89.

MITRA, S. & MOUNT, V. S. 1998. Foreland Basement-cored structures. *American Association of Petroleum Geologists Bulletin* **82**, 70–109.

NARR, W. & SUPPE, J. 1994. Kinematics of basement-cored compressive structures. *American Journal of Science* **294**, 802–60.

NEWBERRY, R. J., SOLIE, D. N., BURNS, L. E., WILTSE, M. A., HAMMOND, W. R. & SWAINBANK, R. 1995. Geophysical and geological evidence for pervasive, northeast-trending left-lateral faults in eastern interior Alaska. *Abstracts with Programs Geological Society of America* **27**, 68.

OTTEMAN, A. S. & SNOKE, A. W. 2005. Structural analysis of a Laramide, basement-cored, foreland fault zone, Rawlins uplift, south-central Wyoming. *Rocky Mountain Geology* **40**, 65–89.

PAYLOR, E. D. II. & YIN, A. 1993. Left-slip evolution of the North Owl Creek fault system, Wyoming, during Laramide shortening. In *Laramide Basement Deformation in the Rocky Mountain Foreland of the Western United States* (eds C. J. Schmidt, R. B. Chase & E. A. Erslev), pp. 229–42. Geological Society of America Special Paper no. 280.

ROYDEN, L. H., BURCHFIEL, C., KING, R. W., WANG, E. C., CHEN, Z. L., SHEN, F. & LIU, Y. P. 1997. Surface deformation and lower crustal flow in Eastern Tibet. *Science* **276**, 788–800.

SCHMIDT, C. J., GENOVESE, P. W. & CHASE, R. B. 1993. Role of basement fabric and cover-rock lithology on the geometry and kinematics of twelve folds in the Rocky Mountain foreland. In *Laramide Basement Deformation in the Rocky Mountain Foreland of the Western United States* (eds C. J. Schmidt, R. B. Chase & E. A. Erslev), pp. 1–44. Geological Society of America Special Paper no. 280.

SCHREURS, G. & COLLETTA, B. 1998. Analogue modeling of faulting in zones of continental transpression and transtension. In *Continental Transpressional and Transtensional Tectonics* (eds R. E. Holdsworth, R. A. Strachan & J. F. Dewey), pp. 59–79. Geological Society of London, Special Publication no. 135.

SPANG, J. H. & EVANS, J. P. 1988. Geometrical and mechanical constraints on basement-cored thrusts in the Rocky Mountain foreland province. In *Interaction of the Rocky Mountain Foreland and the Cordilleran Thrust Belt* (eds C. J. Schmidt & W. J. Perry), pp. 41–51. Geological Society of America Memoir no. 171.

STEARNS, D. W. 1978. Faulting and forced folding in the Rocky Mountains foreland. In *Laramide Folding Associated with Block Faulting in the Western United*

States (ed. V. Matthews), pp. 1–37. Geological Society of America Memoir no. 151.

STONE, D. S. 1993. Basement-cored thrust-generated folds as seismically imaged in the subsurface of the central Rocky Mountain foreland. In *Laramide Basement Deformation in the Rocky Mountain Foreland of the Western United States* (eds C. J. Schmidt, R. B. Chase & E. A. Erslev), pp. 271–318. Geological Society of America Special Paper no. 280.

STONE, D. S. 2002. Morphology of the Casper Mountain uplift and related, subsidiary structures, central Wyoming: implications for Laramide kinematics, dynamics, and crustal inheritance. *American Association of Petroleum Geologists Bulletin* **79**, 1417–40.

TAPPONNIER, P., XU, Z. Q., ROGER, F., MEYER, B., ARNAUD, N., WITTLINGER, G. & YANG, J. S. 2001. Oblique stepwise rise and growth of the Tibet Plateau. *Science* **294**, 1671–7.

TINDALL, S. E. & DAVIS, G. H. 1999. Monocline development by oblique-slip fault-propagation folding: the East Kaibab monocline, Colorado Plateau, Utah. *Journal of Structural Geology* **21**, 1303–20.

TU, D. L., WANG, Z. J., ZENG, B. H. & GAO, Q. 1998. Study on distribution and activity characters of the Holocene faults in the Huangshui Basin, Qinghai Province. *Northwestern Seismological Journal* **20**, 83–90 (in Chinese with English abstract).

VARGA, R. J. 1993. Rocky Mountain foreland uplifts: products of a rotating stress field or strain partitioning? *Geology* **21**, 1115–8.

WANG, X. L., LU, Y. C. & LI, X. N. 2005. Luminescence dating of fine-grained quartz in Chinese loess: simplified multiple aliquot regenerative dose (MAR) protocol. *Seismology and Geology* **27**, 615–22 (in Chinese with English abstract).

WANG, J. S., ZHANG, K. C., WANG, Z. C. & BAI, Y. S. 2006. Analysis on relationship between the deep geological structure and earthquakes in Xining Basin. *Earthquake Research in Plateau* **18**, 16–24 (in Chinese with English abstract).

WISE, D. U. & OBI, C. M. 1992. Laramide basement deformation in an evolving stress field, Bighorn Mountain front, Five Springs area, Wyoming. *American Association of Petroleum Geologists Bulletin* **76**, 1586–600.

YIN, A., DANG, Y. Q., ZHANG, M., CHEN, X. H. & MCRIVETTE, M. W. 2008. Cenozoic tectonic evolution of the Qaidam basin and its surrounding regions (Part 3): structural geology, sedimentation, and regional tectonic reconstruction. *Geological Society of America Bulletin* **120**, 847–76.

YIN, G. M., ZHAO, H., YIN, J. H. & LU, Y. C. 2002. Chronology of the stratum containing the skull of the Dali Man. *Chinese Science Bulletin* **47**, 1302–7.